Beyond BioID: Streptavidin outcompetes antibody fluorescence signals in protein localization and readily visualises targets evading immunofluorescence detection

Johanna Odenwald[1], Bernardo Gabiatti[1], Silke Braune[1], Siqi Shen[2], Martin Zoltner[2*] and Susanne Kramer[1*]

[1] Biocenter, University of Würzburg, Würzburg, Germany

[2] Department of Parasitology, Faculty of Science, Charles University in Prague, Biocev, Vestec, Prague, Czech Republic

* corresponding authors

Tel.: +49 931 3186785

Email: susanne.kramer@uni-wuerzburg.de

Email: martin.zoltner@natur.cuni.cz

short title: Imaging applications of TurboID

ABSTRACT

Immunofluorescence is a common method to localise proteins within their cellular context via fluorophore labelled antibodies and for some applications without alternative. However, some protein targets evade detection due to low protein abundance or accessibility issues. In addition, some imaging methods require a massive reduction in antigen density thus impeding detection of even medium-abundant proteins.

Here, we show that the fusion of the target protein to TurboID, a biotin ligase labelling lysine residues in close proximity, and subsequent detection of biotinylation by fluorescent streptavidin offers an “all in one” solution to the above-mentioned restrictions. For a wide range of target proteins tested, the streptavidin signal was significantly stronger than an antibody signal, markedly improving the imaging sensitivity in expansion microscopy and correlative light and electron microscopy, with no loss in resolution. Importantly, proteins within phase-separated regions, such as the central channel of the nuclear pores, the nucleolus or RNA granules, were readily detected with streptavidin, while most antibodies fail to label proteins in these environments. When TurboID is used in tandem with an HA epitope tag, co-probing with streptavidin and anti-HA can be used to map antibody-accessibility to certain cellular regions. As a proof of principle, we mapped antibody access to all trypanosome nuclear pore proteins (NUPs) and found restricted antibody labelling of all FG NUPs of the central channel that are known to be phase-separated, while most non-FG Nups could be labelled. Lastly, we show that streptavidin imaging can resolve dynamic, temporally and spatially distinct sub-complexes and, in specific cases, reveal a history of dynamic protein interaction.

In conclusion, streptavidin imaging has major advantages for the detection of lowly abundant or inaccessible proteins and in addition, can provide information on protein interactions and biophysical environment.

INTRODUCTION

Visualisation of a protein within the cellular context is routinely achieved either by fusing it to a fluorescent protein, or by using fluorophore labelled antibodies specific for a target protein or peptide tag that is genetically fused to it. Fluorescent proteins are not suitable for all imaging applications, because fluorescence is lost under fixation and permeabilization conditions. Applications that are fully dependent on antibodies include correlative electron and light microscopy (CLEM) applications, expansion microscopy or protein detection in combination with *in situ* hybridisation for nucleic acid detection.

Sometimes, antibodies fail to detect a protein at its expected localisation, which is rarely followed up or reported. We recently observed the absence of an anti-HA antibody signal at the nuclear pores for endogenously expressed trypanosome mRNA export factor MEX67 fused to the small peptide hemagglutinin (HA) epitope tag: the anti-HA signal was entirely restricted to the nucleoplasm (Moreira et al., 2023). Likewise, a polyclonal antibody raised against *T. brucei* MEX67 did not stain the nuclear pores (Pozzi et al., 2023). In contrast, fusions of *T. brucei* MEX67 to fluorescent proteins (either N- or C-terminally) are primarily detected at the nuclear pores with some signal extending to the nucleoplasm (Billington et al., 2023; Kramer et al., 2010). This is in agreement with the reported function of *T. brucei* MEX67 in mRNA export (Dostalova et al., 2013; Schwede et al., 2009) and with nuclear pore localisation of MEX67 orthologues in other eukaryotes (Katahira et al., 1999; Köhler and Hurt, 2007; Mangus et al., 2003; Rodriguez et al., 2004; Stewart, 2019; Sträßer et al., 2000; Terry and Wente, 2007) where Mex67 was even termed a mobile nucleoporin (Derrer et al., 2019). We next expressed *Tb*MEX67 fused to a TurboID-HA tandem tag. TurboID is a biotin ligase, widely employed for proximity labelling techniques facilitating analysis of protein interactions *in vivo* (Branon et al., 2018). To our surprise, fluorophore labelled streptavidin readily delivered a signal localizing primarily to the nuclear pores and partially to the nucleoplasm, consistent with the localisation of MEX67 fused to fluorescent proteins (Moreira et al., 2023). We therefore concluded that the streptavidin signal shows the correct localization of MEX67, while antibodies fail to bind MEX67 at the nuclear pore and selectively stain the nucleoplasmic fraction of MEX67. One possible reason for the absence of antibody stain could be the localisation of MEX67 to the central channel of the nuclear pore that is lined by phenylalanine-glycine nucleoporins (FG NUPs), intrinsically disordered proteins dominated by FG-repeats,

that assemble to a dense meshwork and create a phase-separated environment, physically distinct from the rest of the cell (Davis et al., 2022; Nag et al., 2022).

Here, we set out to investigate whether streptavidin imaging offers a general solution to antibody-accessibility problems. We expressed 11 trypanosome and one mammalian protein of different *bona fide* phase-separated regions (nucleolus, stress granules, central channel of the nuclear pores) fused to a TurboID-HA tandem tag. All proteins could be readily visualised with streptavidin, while they could not be labelled with anti-HA. Importantly, we noticed that streptavidin imaging has further major advantages to antibody labelling, even for antibody-accessible proteins: (i) the multiple biotinylation sites of the bait and adjacent proteins provided a massive boost in signal, which is in particular useful in applications with diluted antigens, such as expansion microscopy or correlative light and electron microscopy (CLEM); (ii) since biotinylation extends to adjacent proteins and is stable over the lifetime of a protein, protein interactions are preserved in time, enabling to monitor dynamic processes in the cell.

MATERIALS and METHODS

Culture and genetic modification of trypanosomes

T. b. brucei Lister 427 procyclic cells were cultured in SDM-79 (Brun and Schönenberger, 1979). Generation of transgenic trypanosomes was performed using standard methods (McCulloch et al., 2004). Almost all trypanosome fusion proteins were expressed from the endogenous locus, by modifying one allele via a PCR-based approach reliant on a (modified) version of the pPOT vector system (Dean et al., 2015). Occasionally, a plasmid-based system was used for endogenous tagging (Kelly et al., 2007). For overexpression of ALPH1-eYFP, a tetracycline inducible system was used (Sunter et al., 2012) and expression was induced for 24 hours. Details about all fusion constructs are provided in Table S1. The TurboID-HA tandem tag encodes the TurboID open reading frame, followed by a two-amino acid long spacer (AS), followed by the HA tag (YPYDVPDYA). The TurboID-Ty1 tandem tag encodes the TurboID open reading frame, followed by a short linker (ASGSGS), followed by the Ty1 tag (EVHTNQDPLD). The 3Ty1-NG-3Ty1 tag, allowing fusion of mNeonGreen (NG) flanked by two triple Ty1 epitopes, originates from the pPOT system (Dean et al., 2015).

Culture and genetic manipulation of HeLa cells

pEGFP-N1 was modified to contain the sequence encoding TurboID-HA with a stop-codon upstream of the eGFP sequence. Sequences of the open reading frames of NUP88 and NUP54 were amplified from human cDNA and cloned in frame downstream of the TurboID-HA sequence. This results in expression of NUP88 or NUP54 fused to the N-terminal TurboID-HA tag, without the eGFP. The sequences of the fusion proteins are provided in Table S1. HeLa cells were grown in Dulbecco's modified Eagle's medium (DMEM; Gibco by Life Technologies, Darmstadt, Germany) supplemented with 10% fetal calf serum (FCS; Capricorn Scientific, Ebsdorfergrund, Germany) and 1% penicillin-streptomycin (Thermo Fisher Scientific, Dreireich, Germany) at 37°C and 5% CO_2. Cells were transfected with the respective TurboID-HA fusion constructs using Effectene™ (Qiagen, Hilden, Germany) following the manufacturer's protocol and incubated for ~24 hours in a petri-dish containing a coverslip. Immunofluorescence/streptavidin labelling was performed on cells attached to the coverslips, as detailed below for trypanosomes.

Immunofluorescence and streptavidin labelling

About 1×10^7 procyclic-form *T. brucei* cells, harvested at a density of 5×10^6 cells/ml, were washed once in 1 ml SDM79 without hemin and serum and resuspended in 500 µl PBS. For fixation, 500 µl of 8% paraformaldehyde was added for 20 min while rotating. After addition of 7 ml PBS supplemented with 20 mM glycine, cells were pelleted, resuspended in 150 µl PBS, and spread on poly-lysine-coated slides (within circles drawn with a hydrophobic pen). Cells were allowed to settle for 15 min, before removing surplus PBS and permeabilizing cells with 0.5% Triton X-100 in PBS. Slides were rinsed in PBS, and cells were then blocked in 3% bovine serum albumin (BSA) in PBS for 30 min, followed by 60 min incubation with rabbit mAb-anti-HA C29F4 (1:500 dilution; Cell Signaling Technology) and Streptavidin-Cy3 (1:200 dilution; Jackson Laboratories) in PBS/3% BSA. Slides were washed in PBS (three times for 5 min), then incubated with anti-rabbit Alexa Fluor Plus 488 (1:500 dilution, A32731 Invitrogen) in PBS/3% BSA for 50 min and a further 10 min upon addition of 4',6-diamidino-2-phenylindole (DAPI) (0.1 µg/ml). Slides were washed 3 × 5 min in PBS and embedded into ProLong Diamond Antifade Mountant (Thermo Fisher Scientific). For control experiments, the following antibodies/nanobodies were used: Ty1-tag monoclonal antibody BB2 (hybridoma supernatant, 1:300); *T. brucei* MEX67 polyclonal antiserum (1:1000, kind gift of Mark Carrington) and anti-GFP nanobody (GFP-Booster Alexa Fluor 647 Chromotek gb2AF647, 1:1000).

Microscopy

For most fluorescence microscopy experiments, images were acquired using a DMI8 widefield microscope (Thunder Imager, Leica Microsystems, Germany) with a HCX PL APO CS objective (100x, NA = 1.4, Leica Microsystems) and Type F Immersion Oil (refractive index = 1.518, Leica Microsystems). The microscope was controlled using LAS-X software (Leica Microsystems). Samples were illuminated with an LED8 light source (Leica). Excitation light was selected by using the following filter sets: Ex 391/32 nm; DC 415nm; Em 435/30 nm (DAPI), 436/28 nm; DC 459 nm; Em 519/25 nm (AlexaFluor™ 488), 554/24 nm; DC 572 nm; Em 594/32 nm (Cy3), 578/24 nm; DC 598 nm; Em 641/78 nm (AlexaFluor™ 594). Images were captured using a K5 sCMOS camera (Leica, 6.5 µm pixel size). Between 50 and 70 images in 140 nm distances were recorded for each Z-stack. Exposure times were 100-200 ms for DAPI and between 200-800 ms for all other fluorophores. For some images, an inverted wide-field microscope Leica DMI6000B (Leica Microsystems GmbH, Wetzlar, Germany)

equipped with a 100x oil immersion objective (NA 1.4) and a Leica DFC365 camera (6.5 µm/pixel) was used. Filter sets were (i) ex: 340–380 nm, dc: 400nm, em: 450–490 nm (DAPI), (ii) ex: 450–490 nm, dc: 495nm, em: 500–550 nm (eYFP), (iii) ex: 530–560nm, dc: 570 nm, em: 572- 648 nm (TMR). Image acquisition was done like on the thunder imager. Images are shown either unprocessed (raw data) or processed by instant computational clearing (Software provided by the Thunder imager) or deconvolution using Huygens Essential software (Scientific Volume Imaging BV). Presentations are either as single plane or as Z-stack projection (sum slices), as indicated. Scanning electron microscopy and correlation with light microscopy was done as previously described (Kramer et al., 2020).

Affinity enrichment of biotinylated proteins and on beads digestion

The isolation of biotinylated proteins from trypanosomes and preparation for mass spectrometry was done as previously described (Moreira et al., 2023), except that 1 mM biotin was added during the elution step from the streptavidin beads by tryptic digest, to improve recovery of biotinylated peptides.

Western blots

Western blotting was performed using standard methods. Detection of biotinylated proteins was done with Streptavidin-IRDye®680LT (LI-COR) (1:20,000). Proteins with HA-tag(s) were detected using rat mAb-anti-HA 3F10 (Roche, 1:1000) as primary antibody and IRDye® 800CW Goat anti-Rat IgG (Licor, 1:20,000) as secondary antibody.

Mass spectrometry and proteomics analysis

TurboID-eluted peptides were resuspended in 50 mM NH_4HCO_3 and passed over C18 stage tip columns as described (Rappsilber et al., 2007) and then analyzed by LC–MS/MS on an Ultimate3000 nano rapid separation LC system (Dionex) coupled to an LTQ Orbitrap Fusion mass spectrometer (Thermo Fisher Scientific). Minimum peptide length was set at seven amino acids allowing a maximum of two missed cleavages, and FDRs of 0.01 were calculated at the levels of peptides, proteins, and modification sites based on the number of hits against the reversed sequence database. Spectra were processed using the intensity-based label-free quantification (LFQ) in MaxQuant version 2.1.3.0 (Cox and Mann, 2008; Cox et al., 2014) searching the *T. brucei* strain TREU927 annotated protein database (version 63) from

TriTrypDB (Aslett et al., 2010). Statistical analyses of LFQ data were done in Perseus (Tyanova et al., 2016). LFQ values were filtered for at least one valid value in the bait sample group, log2 transformed and missing values imputed from a normal distribution of intensities around the detection limit of the mass spectrometer. These values were subjected to a Student's t-test comparing the respective bait sample groups to an untagged control (wt parental cells) triplicate sample group. The resulting *t*-test difference is the difference between the means of logarithmic abundances of a protein group. Bait samples were prepared in duplicate (NUP76, NUP96, NUP110) or triplicate (MEX67, NUP158). All proteomics data have been deposited at the ProteomeXchange Consortium via the PRIDE partner repository (Perez-Riverol et al., 2019) with the dataset identifier PXD031245 (MEX67, NUP158, wt control, GFP control) and PXD047268 (NUP76, NUP96, NUP110).

Ultrastructural Expansion Microscopy (U-ExM) with procyclic T. brucei

The U-ExM method was performed as described in (Gambarotto et al., 2020) with some modifications. $1x10^7$ trypanosome cells were harvested (1500 g, 10 min) and the pellet resuspended in 500 µl PBS. 500 µl 8% formaldehyde (FA, 36.5-38%, F8775, Sigma)/8% acrylamide (AA, 40%, A4058, Sigma) diluted in PBS was added to achieve a final concentration of 4%FA/4%AA. Cells were allowed to settle on a 12 mm round coverslip treated with poly-L-lysine (P8920, Sigma) placed in a well of a 24-well plate. The adjacent wells were filled with ddH_2O, the plate sealed with parafilm and incubated at 37°C for 5 hours. A small piece of parafilm was placed on top of a humid chamber, where a drop of monomer solution (sodium acrylate 23% (w/v) (408220, Sigma), AA 10% (w/v), N-N'-methylenebisacrylamide 0.1% (w/v) (M7279, Sigma) in PBS) was added. The coverslip was placed on top of the drop, with the cells facing down. The coverslip was removed, cleaned from excess liquid with a laboratory wipe and placed in 40 µl of monomer solution freshly complemented with 1 µl 10% APS (327085000, Acros Organic) and 1 µl 10% TEMED (T7024, Sigma). Sodium acrylate stock solution 38% (w/v) was prepared by dissolving 1.9 g sodium acrylate in 3.1 ml of ddH_2O followed by filtering through 0.2 µm filter. The humid chamber was closed, and the gel allowed to polymerize for one hour at 37°C. Coverslips were transferred to a well of a 6-well plate containing 1 ml denaturation buffer (200 mM SDS (A1112, Applichem), 200 mM NaCl (A2942, Applichem) and Tris-HCl pH 9 (5429.3, Roth)) and incubated for 15 minutes with gentle shaking. Gels were detached from the coverslips with a spatula and transferred to a 1.5 mL

Eppendorf tube. The tube was filled with denaturation buffer to the top, closed and incubated at 95°C for 90 minutes in a heating block. Gels were transferred to a beaker with 100 ml ddH_2O for the first round of expansion for 30 minutes. Water was exchanged and two more rounds of expansion were done, the last one being overnight at room temperature. The next day, gels were carefully transferred to a Petri dish and imaged to measure the expansion factor. Gels were transferred to a fresh beaker containing 100 ml PBS and incubated for 15 minutes. This was repeated once and then the gel was trimmed to a square of about 12 x 12 mm which was transferred to a 24-well plate for antibody incubation. Gels were incubated with 0.5 ml PBS BSA 3% (A1391, Applichem) with primary antibodies (mouse-anti-HA monoclonal antibodies (C29F4, Cell Signaling) at 1:500) at 37°C for three hours in a plate shaker at 1500 RPM. Gels were transferred to a 6-well plate for washing. They were washed three times with 10 ml PBS-T (0.1% Tween20 in PBS) for 10 minutes with agitation at room temperature. Gels were transferred back to a 24-well plate and incubated with 0.5 ml PBS BSA 3% with secondary antibodies AlexaFluor™ 488 goat anti-rabbit (A11008, Sigma, 1:500), Cy3-streptavidin and 0.1 µg/ml DAPI (D9542, Sigma) at 37°C for three hours in a plate shaker at 1500 RPM. Gels were transferred to the 6-well plate and washed four times with 10 ml PBS-T for 10 minutes with agitation at room temperature, all steps from now on protected from light. Gel pieces were expanded again in 100 ml ddH_2O in a beaker, with three water exchanges each 30 minutes and the last expansion step done overnight at room temperature. An imaging chamber Nunc™ Lab-Tek™ II with one chamber (734-2055, Thermofisher Scientific) was covered with a layer of poly-D-lysine (A3890401, Gibco) for one hour and left to dry overnight. For imaging, the gel pieces were trimmed to fit the chamber, excess water was removed with a laboratory wipe and the gel was placed in the imaging chamber, taking care not to shift after the initial placement. A drop of water was added to cover the top of the gel. The gel chamber was closed with the lid to avoid evaporation during imaging. For longer imaging sessions, drops of water were periodically added to prevent gel drying. Since cells can be on either side of the gel, the gel was divided into two pieces, one facing up and one facing down, to ensure cells can be detected, on either piece.

Protein retention Expansion Microscopy (proExM) in procyclic T. brucei

The proExM method was performed as described in (Tillberg et al., 2016) with some modifications. $5x10^7$ cells were harvested by centrifugation at 1500 g for 10 minutes, washed

once in 10 ml PBS and finally resuspended in 1 ml of PBS. 1 ml of PFA 8% (P6148, Sigma) was added and cells were fixed for 20 minutes at room temperature with rotation. 13 ml 20 mM glycine (50046, Sigma) in PBS (freshly prepared from a 2M stock) was added to quench and cells were harvested at 1500 g for 10 minutes. Cells were resuspended in 1 ml PBS and let to adhere to a 12 mm coverslip, previously treated with poly-L-lysine, placed in a well of a 24 well plate for 15 minutes. The well was rinsed with PBS and the coverslip incubated with PBS 0.5% Triton for 5 minutes for permeabilization. Wells were rinsed again with PBS and coverslips incubated with PBS 3% BSA for 30 minutes for blocking. 50 µl of primary antibody solution (rabbit anti-HA monoclonal antibodies (C29F4, Cell Signaling) 1:50 diluted in PBS BSA 1%) were placed on a piece of parafilm in a humid chamber and the cover slip was placed on top (cells facing down) for one hour in a humid chamber. The coverslip was returned to the well of the 24 well plate, cells facing up, and wells were washed with PBS (3 x 5 min) with agitation. 250 µl secondary antibodies (streptavidin-Cy3 (SA1010, Sigma) 1:1000; AlexaFluor™ 488 goat anti-rabbit (A11008, Sigma) 1:250) and DAPI ((D9542, Sigma) 1:1000) were added, diluted in 250 µl PBS BSA 1%. Wells were washed with PBS (4 x 5 min). From now on, all steps were done protected from light. To anchor the proteins to the gel, we prepared a solution of 5 mg AcX (Acryloyl-X, SE, 6-((acryloyl)amino)hexanoic Acid, Succinimidyl Ester, A20770, Invitrogen) in 500 µl anhydrous DMSO (D12345, Invitrogen); AcX solution was opened and aliquoted in a desiccated environment at – 20°C. AcX was diluted 1:100 in PBS, a drop was placed on a piece of parafilm in a humid chamber, the coverslips were placed top-down into the AcX drop and incubated at room temperature for 16 hours. Coverslips were returned to a well of a 24 well plate, washed twice for 5 minutes with PBS and stored in the fridge until the end of the day.

Monomer solution was prepared with sodium acrylate 8.6% (w/v) (408220, Sigma), AA 2.5% (w/v), N-N'-methylenebisacrylamide 1.5% (w/v) (M7279, Sigma) and NaCl 11.7% (w/v) (AM9760G, Ambion) in PBS; sodium acrylate stock solution 33% (w/v) was freshly prepared by dissolving 1.9 g sodium acrylate in 5 ml of ddH_2O, 0.2 µm-filtered. For gelation, gelling solution was prepared from 100 µl monomer solution, 1 µl 10% APS and 1 µl 10% TEMED, vortexed and used instantly. 50 µl of gelling solution was placed on a piece of parafilm in a humid chamber; the coverslips were placed on top, cells facing downwards, and incubated at

37°C for one hour. After polymerization, coverslips with the gel attached were transferred to a well of a 6-well plate with 1 ml of digestion solution (0.5% Triton X100, 1 mM EDTA pH 8 (AM9260G, Ambion), 50 mM Tris pH 8 (AM9855G, Ambion) and 1 M NaCl (AM9760G, Ambion) freshly supplemented with 10 µl proteinase K (P8107S, New England Biolabs). Plates were stored slightly tilted to ensure the coverslip was completely covered with digestion solution and incubated at room temperature overnight. Next day, gels were either already detached from the coverslip or could be easily detached with a spatula. Gels were transferred to a Petri dish and three rounds of expansion, each with 20 ml ddH_2O for 20 minutes, were done. After this, a picture was taken to measure the expansion factor. Gel mounting in the imaging chamber and imaging were done as described for UExM.

RESULTS

1. TurboID-fusion proteins can be accurately localised with fluorescent streptavidin by light microscopy

To establish a robust imaging system for TurboID fusion proteins by streptavidin, we expressed the *T. brucei* nuclear pore proteins NUP110, NUP76 and NUP96 fused to a TurboID-HA tandem tag in procyclic *Trypanosoma brucei* cells using both N and C-terminal fusion for each respective target protein. The tag is composed of the biotin ligase TurboID (Branon et al., 2018) and the HA peptide tag. Expression was constitutive from the endogenous locus and labelling relied on the biotin substate present in the medium (0.8 µM in SDM79) (Moreira et al., 2023)Biotinylated proteins were purified by streptavidin affinity and analysed by liquid chromatography coupled to tandem mass spectrometry (LC-MSMS), using both, wild type cells and cells expressing TurboID-GFP for background correction (Moreira et al., 2023). For each bait protein, we quantified and visualised the biotinylation of all other nuclear pore proteins and known transport factors in *t*-test difference increments (Figure 1A, Figure S1, Table S2). Additionally, we reanalysed previously published data of C-terminally tagged MEX67 and NUP158 in the same way ((Moreira et al., 2023), Figure 1A, Figure S1, Table S2)). Neither of the bait proteins caused biotinylation of the entire pore complex. Instead, we observed highly specific labelling patterns for each bait. While the central NUP96 biotinylated most nuclear pore proteins with the marked exception of the nuclear basket, NUP158 and NUP76 caused biotinylation of specific sub-complexes of the pore and MEX67 labelled NUPs lining the channel of the pore (Moreira et al., 2023). The data show that the labelling radius of TurboID, under these conditions, is below the size of the nuclear pore and thus well below the resolution of light microscopy.

Next, we imaged cells expressing nuclear pore proteins fused to the TurboID-HA tandem tag using both cy3-streptavidin and anti-HA in combination with a secondary antibody coupled to the Alexa488 fluorophore (Figure 1B). For *T. brucei* NUP132-TurboID-HA, no obvious differences in resolution were observed between antibody-based and streptavidin-based detection (Figure 1C). Likewise, for human NUP88, expressed as N-terminal TurboID-HA fusion protein in HeLa cells, grown in DMEM medium (relying on the biotin of the serum supplement with a low nanomolar concentration), the signal of anti-HA and of streptavidin appeared

328 highly similar (Figure 1D). The data demonstrated that imaging of Turbo-ID fusion proteins via
329 streptavidin is a reliable alternative, with a resolution that is indistinguishable from antibody-
330 based immunofluorescence in standard light microscopy, which is in agreement with
331 published data on experimentally determined BioID labelling radii (Branon et al., 2018; Kim et
332 al., 2016).
333
334 **2. TurboID-fusion proteins can be imaged in phase separated/protein-dense regions**
335 We had previously expressed one of the *T. brucei* nuclear mRNA transporters, *Tb*MEX67, fused
336 to TurboID-HA and observed that anti-HA failed to stain MEX67 at the nuclear pores, indicating
337 a possible failure of the antibody to either penetrate phase separated areas or to bind the
338 epitope in this environment (details in introduction, (Moreira et al., 2023), Figure 2A).
339 To test this hypothesis, we focussed on two additional *bona fine* phase-separated regions: the
340 nucleolus and starvation stress granules. We expressed a C-terminal TurboID-HA fusion of the
341 trypanosome nucleolar GTP-binding protein NOG1 (Tb927.11.3120) (Billington et al., 2023).
342 The resulting streptavidin signal was exclusively at the nucleolus, which is tractable as distinct
343 compartment within the nucleus lacking DAPI fluorescence (Figure 2B). In contrast, the HA-
344 signal showed no obvious accumulation in the nucleolus and was extremely weak with a
345 patchy distribution throughout the entire cell body, indicating an unspecific background stain
346 (Figure 2B). Thus, just like MEX67, the nucleolar protein NOG1 is detectable by streptavidin,
347 but not by anti-HA immunofluorescence. Next, we starved trypanosome cells that were
348 expressing the established starvation stress granule marker PABP2 (Fritz et al., 2015; Kramer
349 et al., 2013) fused to TurboID-HA and probed the cells with the streptavidin anti-HA
350 combination. Both anti-HA and streptavidin readily detected starvation stress granules (Figure
351 2C). However, the granules detected by anti-HA were in general less distinct and appeared
352 larger than those detected by streptavidin. Indeed, intensity profiles drawn through Z-stack
353 projections of stress granules were 1.4±0.2 -fold wider for anti-HA detection in comparison to
354 streptavidin detection and the corresponding HA profiles frequently exhibited a double-peak
355 (Figure 2D and E). The data are consistent with anti-HA preferentially staining the periphery
356 of the granules, while streptavidin diffuses into and binds within these dense, phase separated
357 particles. A switch of the two fluorophores (Cy3 and Alexa488) gave identical results,
358 controlling for microscopy artefacts as a reason for the differences (Figure S2). Direct eYFP-
359 fluorescence intensity profiles of granules from cells expressing PABP2-eYFP resembled those

of the streptavidin stain, ruling out a preferential granule-peripheral localisation of PABP2 as an explanation (Figure S3). Thus, anti-HA fails to label three distinct phase-separated structures of the trypanosome cell, the nuclear pore channel, the nucleolus and the inside of starvation stress granules, while streptavidin faithfully decorates all these structures.

The inability of anti-HA to detect target epitopes within phase-separated areas is not restricted to trypanosomes: When expressing TurboID-HA fusions of the human FG-repeat nucleoporin NUP54 in HeLa cells, streptavidin detected the proteins at the nuclear pores, while no specific anti-HA signal was observed (Figure 2F).

Furthermore, the inability to label phase-separated areas is not restricted to anti-HA but applies to other antibodies. We expressed *T. brucei* MEX67 and NOG1 fused to TurboID-Ty1 and failed to label the nuclear pores and the nucleolus with anti-Ty1 (BB2), respectively, while the streptavidin signal displayed the correct localisations (Figure 2G and H). Moreover, MEX67 was undetectable by polyclonal antiserum (Figure 2I; (Pozzi et al., 2023)) and an eGFP-fusion of MEX67 could not be detected by fluorophore labelled eGFP nanobodies (Figure 2J). In contrast, an eGFP fusion of NOG1 was detectable by eGFP nanobodies at the nucleolus, albeit weakly (Figure 2J). Also, when NOG1 was fused to mNeongreen flanked on either site by three Ty1-epitope sequences, anti-Ty1 solely detected the periphery of the nucleolus, but failed to stain the centre (Figure 2K). In conclusion, most but not all antibodies/nanobodies were ineffective in phase separated areas.

3. Boosting the signal under low-antigen conditions (expansion microscopy, CLEM)

A potential advantage for imaging TurboID fusion proteins with streptavidin is an increased signal: TurboID is expected to cause multiple lysine-biotinylation of both the bait protein and proteins in close proximity, while antibodies only decorate several (polyclonals) or one specific (monoclonals) epitope of a target protein. Indeed, for many TurboID-HA fusion proteins that we analysed by standard light microscopy, the streptavidin signal appeared significantly stronger and devoid of background stain when comparing to anti-HA. To quantify this observation, we probed cells expressing NUP158-TurboID-HA with combinations of anti-HA/Alexa488 secondary antibody and Streptavidin-Cy3 (Figure 3A) or with Streptavidin-Alexa488 and anti-HA/Alexa594 secondary antibody (Figure 3B). Under both labelling conditions, the streptavidin stain resulted in significantly less non-specific cytoplasmic background signal than anti-HA (Figure 3A-B). Moreover, the maximum Alexa488 signal of Z-

stack projections was 2.9-fold higher for streptavidin than for anti-HA (N=60, unpaired two-tailed *t*-test=9.6E-55) (Figure 3C). An increase in fluorescence signal is desirable for the detection of low abundance proteins, but also for imaging applications that necessitate a reduction in antigen density, such as expansion microscopy or CLEM.

In expansion microscopy, biomolecules are covalently cross-linked to a hydrogel, that is subsequently swollen by osmosis, causing a physical magnification of the sample (Chen et al., 2015). Even a relatively small expansion factor of 3 causes a 27-fold increase in sample volume and thus a 27-fold decrease in antigen-density. The two main expansion microscopy methods are Protein-retention Expansion Microscopy (proExM) (Tillberg et al., 2016) and Ultra-structural Expansion Microscopy (U-ExM) (Gambarotto et al., 2019). The main difference is that in proExM, antibody labelling is applied prior to the expansion process, while in U-ExM it is done afterwards. U-ExM thus generally results in higher resolution, as the linkage-error (difference between position of the fluorophore of the secondary antibody and the position of the target protein) is not expanded. Next to the decrease in antigen-density as a consequence of the expansion, the signal is further compromised by the harsh conditions associated with the method, as for example an incubation step at 95°C in alkaline SDS-containing buffer for 90 min for U-ExM and an over-night proteinase K digestion for ProExM. To assess the potential of streptavidin imaging, we employed both proExM and U-ExM on cell lines expressing TurboID-HA fusions of two trypanosome nuclear-pore localised proteins (NUP76 and MEX67) and compared the signals from streptavidin and anti-HA (Figure 3D). For both proteins, streptavidin caused a strong and uniform stain of all nuclear pores with both expansion microscopy methods. In contrast, anti-HA failed to detect nuclear pores either completely (MEX67) or partially (NUP76) in U-ExM. In proExM, pores could be stained evenly with anti-HA, but the signal was much lower in comparison to streptavidin, in particular for NUP76. To our knowledge, this is the first time that streptavidin imaging of a biotin ligase-fused protein was used in combination with expansion microscopy. In our hands, streptavidin clearly outperformed antibodies in both expansion protocols and with both target proteins that we tested, giving a significantly stronger signal with less background.

CLEM causes an even larger reduction in accessible antigen than expansion microscopy. Thin slices of a resin-embedded sample are first used for immunofluorescence and imaged by light

424 microscopy, and, in a second step, imaged by electron microscopy. The resin largely prevents
425 antibody penetration and probing is therefore restricted to the small fraction of antigens
426 present at the surface of the resin slice. Trypanosome cells expressing NUP96-TurboID-HA or
427 NUP158-TurboID-HA were embedded in LR-white and slices were probed with streptavidin
428 and anti-HA. For both proteins, the streptavidin signal detected numerous pores for each
429 nucleus, while anti-HA detected between 0 and 2 pores and, in addition, caused considerably
430 higher background signals (Figure 3E and Figure S4 in Supplementary materials). Streptavidin
431 is thus more suitable for CLEM, and an example, targeting NUP158-TurboID-HA with both
432 steps, is shown in Figure 3F.
433
434 In summary, streptavidin detection causes a massive increase in signal that is in particularly
435 beneficial under low-antigen density conditions, and thus offers significant implications in
436 expansion microscopy and CLEM.
437
438 **4. Visualization of protein interactions**
439 We found that in most cases, streptavidin labelling faithfully reflects the steady state
440 localisation of a bait protein, e.g., the localisation resembles those observed with
441 immunofluorescence or direct fluorescence imaging of GFP-fusion proteins. For certain bait
442 proteins, this is not the case, for example, if the bait protein or its interactors have a dynamic
443 localisation to distinct compartments, or if interactions are highly transient. It is thus essential
444 to control streptavidin-based *de novo* localisation data by either antibody labelling (if possible)
445 or by direct fluorescence of fusion-proteins for each new bait protein. However, any additional
446 signal from biotinylated partner proteins at a different location can also be leveraged to gain
447 relevant information on the function and dynamics of the bait protein. Three respective
448 examples are detailed below:
449
450 The first is PABP2, one of two trypanosome poly(A) binding proteins, that has established,
451 unambiguous cytoplasmic localisation, when visualised with either anti-HA or when expressed
452 fused to a fluorescent protein (Figure 4A-B, (Billington et al., 2023; Kramer et al., 2013).
453 However, when PABP2-TurboID-HA expressing cells are probed with streptavidin, a signal at
454 the posterior pole of the cell is observed, in addition to the expected cytoplasmic signal (Figure
455 4A). Localisation to the posterior pole is an exclusive feature of the trypanosome mRNA

456 decapping enzyme ALPH1 and its four interaction partners: a small proportion of this mRNA
457 decapping complex localises to the posterior pole, in a dynamic manner, while the majority
458 remains cytoplasmic (Kramer, 2017; Kramer et al., 2008; Kramer et al., 2023) (Figure 4B). The
459 streptavidin signal at the posterior pole of the PABP2-TurboID-HA cells thus likely reflects a
460 historic cytoplasmic interaction between PABP2 and the mRNA decapping complex. The
461 existence of this interaction is supported by the identification of all five posterior-pole
462 localised members of the decapping complex by mass spectrometry data from a PABP2 BioID
463 experiment (Moreira et al., 2023). Notably, imaging with streptavidin adds information about
464 protein dynamic interactions, that mass spectrometry data alone cannot uncover. In this case,
465 it shows that the fraction of mRNA decapping proteins at the posterior pole is dynamically
466 exchanged with the fraction in the cytoplasm.
467
468 The second example is MLP2 (also called NUP92), a divergent nucleoporin of Kinetoplastida
469 involved in chromosome distribution during mitosis (Holden et al., 2014; Morelle et al., 2015).
470 MLP2 localisation is cell cycle dependent: while exhibiting a nuclear localisation during
471 interphase, it migrates to the spindle and spindle pole during mitosis (Holden et al., 2014;
472 Morelle et al., 2015) (Figure S5). We expressed MLP2 fused to an N-terminal TurboID-HA tag
473 and examined the streptavidin and HA signal in interphase and mitotic cells (Figure 4C). Note
474 that in trypanosomes the kinetoplast (mitochondrial DNA, visible as small dot in DAPI stain)
475 divides prior to the nucleus and numbers and positions of kinetoplasts and nuclei are
476 established markers for cell cycle stages (Sherwin and Gull, 1989). We observed that the
477 streptavidin signal “lacked behind” the anti-HA signal at all cell cycle stages. This is most
478 obvious in anaphase, when anti-HA exclusively stains the spindle pole body, while streptavidin
479 decorates both, the nuclei and the spindle pole body. Thus, for proteins with cell-cycle
480 dependent localisation, streptavidin-labelling provides information on both, the previous
481 localisation(s) of the bait, in addition to its current position.
482
483 The third example are nuclear pore proteins. For all NUPs that we tested, we observed the
484 expected streptavidin signal at the nuclear pores (see below). However, for some NUPs, for
485 example NUP65, we observed additional cytoplasmic streptavidin stain that is absent for
486 others, as for example NUP75 (Figure 4 D-E). There were also differences in the amount of
487 nucleoplasmic biotinylation between NUPs. For example, NUP75 showed more nuclear

488 labelling than NUP65 (Figure 4 D-E). The likeliest explanation is, that some NUPs are contacting
489 and thus proximity-labelling proteins in transit. The streptavidin stain in the nucleoplasm or
490 cytoplasm thus provides information about the functions of the individual NUPs in protein
491 import or export, respectively.
492
493 **5. A phase-separation map of the *T. brucei* nuclear pore**
494 We reasoned that our findings that all phase-separated regions of trypanosomes that we
495 tested are inaccessible to anti-HA can be exploited as a tool for de novo identification of
496 phase-separated regions. As a proof of principle, we employed streptavidin-imaging to
497 produce a map of antibody-inaccessible regions of the entire trypanosome nuclear pore
498 complex. We endogenously expressed all known trypanosome nuclear pore proteins fused to
499 TurboID-HA from one allele. For each protein, two cell lines were constructed, one with
500 TurboID-HA fused to the C-terminus, and one with the tag at the N-terminus. We excluded
501 Mlp2/Nup92, as we found this protein localizing to the nucleus rather than the nuclear pores
502 in most interphase cells (Figure S5 in Supplementary material and Figure 4C), in agreement
503 with (Morelle et al., 2015). For two C-terminal fusion candidate proteins (Sec13, NUP140) and
504 one N-terminal (NUP82), we repeatedly failed to obtain cell lines. The remaining 45 cell lines
505 were controlled by western blot probed with anti-HA to confirm the correct size of the fusion
506 protein (Figure S6). Next, cells from all cell lines were probed with anti-HA and fluorescent
507 streptavidin. All cell lines showed streptavidin signal predominantly at the nuclear pores,
508 proving the correct localisation of the fusion proteins (Figure 5A). For N-terminally tagged
509 NUP64 we also observed between one and two streptavidin dots in the nucleus, consistent
510 with the localisation of eYFP-NUP64 in life cells (Billington et al., 2023); a likely mislocalisation.
511 When evaluating the HA signal at the nuclear pores, we observed no antibody stain for the
512 NUPs lining the central channel, while most NUPs at the periphery of the channel were
513 accessible to the antibody (Figure 5). Importantly, there is no correlation between protein
514 abundancy, as determined by proteomics (Tinti and Ferguson, 2022), and
515 immunofluorescence signal, ruling out low antigen abundance as the reason for its absence
516 (Figure S7). All the FG-NUPs of the inner channel (which are known to phase-separate) were
517 among the non-accessible proteins, supporting the idea that the crucial determinant
518 preventing anti-HA detection is mainly or entirely phase separation. Likewise, the mRNA-
519 interacting NUP76 complex consisting of NUP76 and the FG NUPs NUP140 and NUP149

appear non-accessible to anti-HA, except when NUP149 is tagged at the N-terminus. The NUP76 interacting protein NUP158 was inaccessible to antibodies when tagged at the N-terminus, but not at the C-terminus: this is consistent with NUP158 being partially phase-separated as it contains FG-repeats exclusively at the N-terminal half. Among the antibody inaccessible proteins were also some non-FG NUPs. These include proteins of the inner ring, NUP181, NUP144, C-terminally tagged NUP225 and N-terminally tagged NUP65, as well as N-terminally tagged proteins of the outer ring, NUP89 and NUP41. Whether the respective termini of these proteins extend into phase separated areas, or whether antibody access is prevented by steric or other hindrances remains unknown.

In conclusion, we here provide an antibody access map of the entire *T. brucei* nuclear pore that includes all bone-fine FG-NUPs in addition to some non-FG NUPs.

DISCUSSION

We here show that the use of the TurboID-HA tandem tag offers an "all in one" solution to antibody-accessibility problems, without compromising resolution or the strength of the signal. Quite the contrary, streptavidin imaging of TurboID-HA tagged proteins facilitates a massive boost in signal, extending the benefits of the method to protein targets with low antigen abundance. Furthermore, the TurboID-HA tag is suitable to probe protein interactions and provide some evidence for phase-separation.

One protocol suits all - streptavidin readily traces biotin proximity labels

Many proteins are not accessible to antibodies in standard immunofluorescence protocols, in particular proteins localized in phase-separated regions. MEX67 could not be detected at the trypanosome nuclear pore by anti-HA, anti-Ty1, anti-Protein A, polyclonal MEX67 antibodies and even nanobodies to mNeonGreen (this work, (Dostalova et al., 2013; Moreira et al., 2023; Pozzi et al., 2023)); likewise, the human Mex67 homologue TAP/Nxf1 evaded detection by antiserum (Bear et al., 1999). HA-fused trypanosome FG-NUPs and the human FG-NUP NUP54 could not be decorated with anti-HA. Trypanosome starvation stress granules could only be labelled at the periphery and nucleolar proteins evaded antibody detection in trypanosomes (Figure 2) and in human cells (Misteli, 2008; Musinova et al., 2011; Sheval et al., 2005; Zatsepina et al., 1997). There are several approaches available to trouble-shoot antigen-accessibility problems (Piña et al., 2022). Pre-extraction steps prior to fixation employing Triton X100, high salt or nucleases proved successful for the detection of mammalian Mex67 homologue TAP/NXF1 (Ben-Yishay et al., 2019; Katahira et al., 1999). Antibody penetration to nucleolar proteins was improved by including protease treatment (Svistunova et al., 2011). Further, fixation by cold methanol instead of paraformaldehyde was reported to increase antibody access to proteins (Neuhaus et al., 1998). However, the search for individual solutions for each problematic antibody/antigen pair is cumbersome and an improvement of antibody access typically comes at the expense of signal loss and/or disruption of cellular morphology (Piña et al., 2022). With streptavidin labelling we present a method that works for every protein (we tested ~30), without compromising cellular morphology and, most importantly, provides a strong signal as significant additional benefit.

In standard light microscopy, streptavidin imaging offers a resolution comparable to labelling with antibodies. The labelling radius of the biotin ligase BirA was estimated to be approximately 10 nm by using the NUP107-160 Y-complex of the mammalian nuclear pore as a molecular ruler (Kim et al., 2014), enabling for example the determination of substructures of P-bodies and stress granules (Youn et al., 2018). It is thus within the range of an average-sized protein and well below the resolution limit of light microscopy. Consistently, cells expressing nuclear membrane associated proteins fused to BirA (or variants as the related BioID2) can be probed by fluorescent streptavidin with resolutions that are undistinguishable from probing with the respective IgG antibodies (Kim et al., 2016; May et al., 2020). For the biotin ligase variant TurboID, which has a massively decreased labelling time, the biotin labelling radius was measured to be in a similar (Branon et al., 2018; Kim et al., 2016) or slightly larger range (May et al., 2020). Importantly, the addition of 50 µM external biotin massively increased the labelling radius, while in the absence of excessive biotin, the labelling radius remained comparable to the labelling radius of BirA (May et al., 2020). In this work, we avoided the addition of additional biotin to the trypanosome medium (the medium contains 0.8 µM biotin) and serum biotin (approximately 2 nM in mammalian serum (Luong and Vashist, 2020)) was the sole source in HeLa cell medium. Our mass spectrometry data of streptavidin-affinity purified proteins with five nuclear pore localised TurboID-fusion proteins demonstrates that the labelling radius is well below the size of the nuclear pore complex under these conditions, and thus in agreement with published data. Even in expansion microscopy, with 3.6 to 4.2 -fold expansion factors, we did not notice any decrease in resolution; in fact, we could resolve NUPs that reside at different positions within the pore (e.g. inner ring vs basket) by labelling one with streptavidin and the other with an antibody and thus obtained sub-NUP imaging resolution (our own unpublished data). Even though, theoretically, BioID *per se* causes a decrease in resolution as biotinylation extends to proteins in close proximity to the bait, this may well be compensated by the lower linkage error when imaging directly via the small, compact-shaped streptavidin-tetramer rather than by a tandem assembly of two large IgG antibodies (Figure 1B).

Streptavidin tracing of biotin proximity labels delivers high signal intensities.

One major benefit of streptavidin imaging was the increase in signal compared to immunofluorescence, caused by multiple biotinylation sites of the bait and adjacent proteins

serving as an enhancer. An increased signal is beneficial for almost all protein-imaging applications, but in particular for low abundance targets. Most strikingly, streptavidin imaging facilitates imaging targets with low densities as a consequence of the imaging method, as in expansion microscopy and CLEM and is applicable to all target proteins that tolerate tag fusion to either terminus. Notably, to the best of our knowledge, this is the first report of the use of streptavidin imaging in expansion microscopy and CLEM and the only alternative approach to immunofluorescence, as denaturing conditions associated with these methods rule out direct imaging of fluorescent tags.

A combination tag as probe for phase separated areas.

A further important application of the TurboID-HA tandem tag is the *de novo* prediction of phase separated areas in cells. The importance of compartmentalization by liquid-liquid phase separation for almost all cellular functions, including DNA and mRNA metabolism (Dai and Yang, 2023), cell division (Ong and Torres, 2020) and development (So et al., 2021) becomes increasingly evident. Aberrant phase separation can cause disease, as for example neurodegenerative disorders (Chakraborty and Zweckstetter, 2023; Tsoi et al., 2023), underlining the relevance of novel tools for identification and characterization of phase separated regions. For individual proteins, phase separation can be predicted in silico using machine learning, with limited, but increasing accuracy (Venko and Žerovnik, 2023). For a defined mixture of molecules, phase separation can be tested in vitro (Alberti et al., 2018; Zhang and Shen, 2023). However, methods to test phase separation in the cellular context are scarce. The correlation between antibody-inaccessibility and phase separation, that we observed in this study, offers the opportunity to use the TurboID-HA tag to probe for phase separation *de novo*. Notably, the streptavidin stain concomitantly provides a convenient intrinsic control to confirm correct localization of the fusion protein. Moreover, proteins with complex localization patterns can be simultaneously detected in both, phase-separated and non-phase separated regions, as we demonstrated for tracing MEX67 to both, the nucleoplasm and nuclear pores (Figure 1A and G). In trypanosomes, all *bona fine* phase-separated regions were inaccessible to anti-HA, namely the nucleolus, starvation stress granules and the FG NUP environment. The data strongly suggest that the absence of an HA immunofluorescence signal correlates with phase-separation. However, we cannot rule out the possibility, that some proteins may be inaccessible to anti-HA for different reasons, as for

example steric hindrance. The latter scenario would equally favor streptavidin over IgG antibodies for target protein binding due to its much smaller dimensions and higher binding affinity. We observed some non-FG Nups to be anti-HA inaccessible, which were mostly NUPs of the inner ring, close to the core of FG NUPs: whether these NUPs localize to phase-separated areas is not known. Importantly, problems to detect phase-separated proteins by antibodies appear conserved across species (Bear et al., 1999; Misteli, 2008; Musinova et al., 2011; Sheval et al., 2005; Zatsepina et al., 1997). We show data for the human FG-NUP Nup54 as an example of an anti-HA-inaccessible protein (Figure 2F) as proof of principle, that the *de novo* identification of phase-separation is applicable to human cells.

Why are most antibodies and, to some extent even fluorophore conjugated nanobodies, prevented from labelling proteins in phase separated environments, while streptavidin never fails? We cannot distinguish whether the lack in labelling is caused by an access problem of the antibody penetrating the phase separated area or by a reduced binding affinity between antibody and antigen in phase-separated environments, or by a combination of both. Still, the smaller size of streptavidin in comparison to an IgG tandem-antibody pair (Figure 1b) likely favors its access into dense regions. Further, IgG antibodies as well as single chain antibodies typically have affinities in the nanomolar range, comparing to femtomolar affinity of the biotin-streptavidin interaction, which is indeed among the strongest non-covalent interactions in nature (Chivers et al., 2011). Together with the extremely high structural stability of streptavidin towards temperature, pH and denaturing conditions (Laitinen et al., 2006) this can explain the ability of this probe to potently outperform antibodies in phase separated environments.

Proximity-labelling reports a history of dynamic protein interactions

Lastly, we propose streptavidin imaging as a novel tool to monitor dynamic interactions between proteins. Since BioID proximity labeling is not restricted to the bait protein, but extends to all interacting partners, the history of interactions is preserved. Hence, changes in protein sub-complexes can be imaged over time. We provide three examples, covering protein complex dynamics in cell cycle regulation and mRNA metabolism as well as nuclear transport. There are many other potential applications. While we relied on an endogenous, constitutive expression of TurboID fusion proteins, a tightly controlled, inducible system, as for example Split-TurboID (Cho et al., 2020) in combination with light activation (Chen et al., 2022; Shafraz

et al., 2023) would allow pulse chase experiment, delivering quantitative data on the kinetics of processes.

Altogether, streptavidin imaging is a highly versatile tool with multiple applications, ranging from a simple boost in signal that can be leveraged to increase imaging sensitivity in expansion microscopy and CLEM, to the ability to probe for phase-separated areas and to monitor dynamic protein interactions. It is thus an important addition to the available imaging toolbox.

ACKNOWLEDGEMENT

The work was financed by a bilateral GACR/DFG grant (project IDs.: 21-19503J and KR4017/9-1; to M. Z. and S. K., respectively). We are grateful to the OMICS Proteomics BIOCEV core facility for excellent technical service. We thank Mark Carrington (University of Cambridge, UK) for providing anti-TbMEX67. Manfred Alsheimer is acknowledged for providing advice and plasmids on HeLa cell transfections, Christian Janzen for the BB2 antibody and Elisabeth Meyer-Natus and Tim Krüger for help with microscopy and image analysis (all University of Würzburg, Germany).

FIGURE LEGENDS

Figure 1: The TurboID biotinylation labelling radius is sufficiently small to allow streptavidin-based imaging of target proteins by light microscopy

A) Schematic representation of the trypanosome NPC (Obado et al., 2016) including selected transport factors and their enrichment observed in TurboID experiments followed by streptavidin affinity capture and LC MS/MS analysis. Proteins quantified are filled in shades of green representative of the corresponding *t*-test difference increments. The respective bait protein is drawn in pink and undetected proteins are in gray. NUP96, NUP76 and NUP110 experiments were analysed with TurboID-HA fusions at both respective termini (as indicated). The nuclear envelope is drawn in sand and nucleoporins and transport factors are numbered in the legend (right) according to (Obado et al., 2016) (NMD3, Tb927.7.970; RanBP1, Tb927.11.3380; RanBPL, Tb927.10.8650; exportin 1, Tb927.11.14340; GAP, Tb927.10.7680),
B) Schematics illustrating the imaging concept for a protein of interest (POI) by either Cy3-streptavidin or anti-HA coupled with secondary Alexa488-labelled antibodies.
(C-D) Nuclear pore proteins of *Trypanosoma brucei* (C) and HeLa cells (D) were expressed fused to the streptavidin-HA tandem tag and detected with streptavidin-cy3 (pink) and anti-HA (green). A representative single plane image of a Z-stack is shown, as raw data (C) or processed by computational clearing (D).

Figure 2: Streptavidin can detect targets within phase-separated regions, while most antibodies fail

(A-B) *T. brucei* MEX67 (A) and *T. brucei* nucleolar protein NOG1 (B) were expressed fused to a C-terminal TurboID-HA tandem tag and cells probed with streptavidin-cy3 (pink) and by anti-HA immunofluorescence (green). Representative single plane images of an unprocessed Z-stack series are shown.
(C-E) Cells expressing the stress granule marker protein PABP2 fused to TurboID-HA were starved (2 hours PBS) and starvation stress granules detected by streptavidin (pink, Cy3) and anti-HA (green, Alexa488). The starvation experiment was performed in biological triplicates. One representative image of starved cells is shown as Z-stack projection (72 slices a 140 nm, sum slices) in C. For each replicate, intensity profiles across one of the larger granules of the cell were measured for 25 cells in both fluorescence channels. The profiles for replicate 1 are

shown in D. For each granule, the granule diameter was calculated from the profiles at 50% fluorescence and the difference in diameter between the HA- and streptavidin stain is presented in E for each replicate, as quotient of granule diameters. Note that despite differences between the three replicates, likely arisen from starvation conditions being not 100% reproducible, the HA stain consistently delivered a larger granule diameter than the streptavidin stain, consistent with preferentially peripheral staining of the granule by anti-HA. For replicate 2, the fluorophores were switched, with essentially the same result (Figure S2 in Supplementary Materials).

(F) Human NUP54 fused to TurboID-HA was expressed in HeLa cells and cells were probed with both anti-HA (green, Alexa488) and streptavidin (Cy3, shown in pink). Streptavidin, but not anti-HA detects NUP54 at the nuclear pores. A single plane image of a Z-stack, processed by computational clearing, is shown.

(G and H) *T. brucei* MEX67 (G) and NOG1 (H) were expressed as TurboID-Ty1 fusion proteins and detected with streptavidin (Cy3, shown in pink) and anti-Ty1 (BB2, green). Representative single plane images of unprocessed Z-stack images are shown.

(I) Trypanosome wild type (WT) cells were probed for MEX67 with polyclonal antiserum (kind gift of Mark Carrington, University of Cambridge; secondary antibody Alexa 488, shown in pink). One representative single plane image of an unprocessed Z-stack image is shown.

(J) *T. brucei* MEX67 (left) and NOG1 (right) were expressed as eGFP fusion proteins and detected with Cy5 labelled eGFP nanobodies. Representative single plane images of unprocessed Z-stack images are shown.

(K) *T. brucei* NOG1 was expressed fused to mNeongreen flanked by three Ty1 epitope tags on either site and detected with anti-Ty1 (secondary antibody Alexa 488; shown in pink).

Figure 3: Streptavidin imaging yields higher signal intensities than immunofluorescence

(A-C) Enhanced signal in standard light microscopy

Trypanosome cells expressing NUP158-TurboID-HA were labelled with combinations of either streptavidin-Cy3 and anti-HA/Alexa488 secondary (A) or with streptavidin-Alexa488 and anti-HA//Alexa 594 secondary (B). Z-stack images were recorded (48 slices a 140 nm). Representative, unprocessed single plane images are shown (A and B). The maximum Alexa488 fluorescence was quantified from Z-stack projections (sum slices) from 60 cells

743 probed with anti-HA or streptavidin; the data are presented as a dot blot (waist is median; box
744 is IQR; whiskers are ± 1.5 IQR) (C)
745 **(D) Improved signal in expansion microscopy**
746 Trypanosome cells expressing NUP76-TurboID-HA or MEX67-TurboID-HA were imaged using
747 Pro-expansion or Ultra-expansion microscopy. Single plane and Z-stack projections (sum
748 slices) of the streptavidin and anti-HA signal are shown for one representative nucleus. All
749 images were deconvolved in proExM, except for NUP76 $_{anti}$-HA.
750 **(E-F) Improved signal in CLEM**
751 Trypanosome cells expressing NUP158-TurboID-HA were embedded in LR-White resin. Slices
752 were probed with streptavidin and anti-HA and imaged by light microscopy (E) followed by
753 electron microscopy (CLEM) (F).
754
755 **Figure 4: Visualisation of protein interactions with TurboID**
756 **(A)** Trypanosome cells expressing PABP2-TurboID-HA were probed with streptavidin and anti-
757 HA. A representative image of the posterior part of a cell is shown (single plane of a Z-stack
758 processed by computational clearing). The position of posterior pole granule is indicated by
759 arrows.
760 **(B)** Trypanosome cells were transformed to co-express PABP2-mChFP and ALPH1-eYFP. A
761 representative image of the posterior part of a cell is shown (single plane of a Z-stack
762 processed by deconvolution). The position of posterior pole granule is indicated by arrows.
763 **(C)** Trypanosome cells expressing TurboID-HA-MLP2 were probed with streptavidin and anti-
764 HA. One representative image of an interphase, prophase, metaphase and an anaphase cell
765 are shown. All images are unprocessed single plane images, with the exception of the DAPI
766 image that is a Z-stack projection (max intensity of 48 slices a 140 nm).
767 **(D and E)** Trypanosome cells expressing NUP65 (D) or NUP75 (E) fused to a C-terminal TurboID-
768 HA tag were probed with streptavidin. Single plane and Z-stack projection (sum slices of 48
769 slices a 140 m) of unprocessed images are shown.
770
771 **Figure 5: A refined map of the *T. brucei* nuclear pore complex**
772 Each known *T. brucei* nuclear pore protein was expressed fused to TurboID-HA, each both at
773 the N- and C-terminus. Cells were labelled with anti-HA and with streptavidin.

774 **(A)** For each NUP, a representative image of the nucleus is shown as unprocessed, single plane
775 of a Z-stack. We evaluated the extent of anti-HA stain in colour increments (shown as a bar
776 above images).
777 **(B)** The HA-signal at the nuclear pores was mapped onto a schematic representation of the
778 trypanosome NPC (modified from (Obado et al., 2016)) using the same colour increments.
779 **(C)** Scheme of the *T. brucei* nuclear pore, with known FG NUPs (Obado et al., 2016) shown in
780 black on the left side and prediction of phase separation (Chu et al., 2022) mapped on the
781 right.
782
783 Figure S1: Statistical analysis of NUP TurboID experiments
784 Figure S2: colour Swap PABP2-TurboID-HA
785 Figure S3: PABP2-eYFP starved and profile
786 Figure S4: LR White probing NUP158, NUP96
787 Figure S5: Mlp2/Nup92, image with many cells, both C and N terminal
788 Figure S6: Western blots Phase ID
789 Figure S7: no correlation between antigen abundance and absence of HA signal
790 Table S1: List of all plasmids used in this work.
791 Table S2: NUP TurboID proteomics data and statistical analysis.
792
793

LITERATURE

Alberti, S., Saha, S., Woodruff, J. B., Franzmann, T. M., Wang, J. and Hyman, A. A. (2018). A User's Guide for Phase Separation Assays with Purified Proteins. *Journal of Molecular Biology* 1–15.

Aslett, M., Aurrecoechea, C., Berriman, M., Brestelli, J., Brunk, B. P., Carrington, M., Depledge, D. P., Fischer, S., Gajria, B., Gao, X., et al. (2010). TriTrypDB: a functional genomic resource for the Trypanosomatidae. *Nucleic Acids Research* **38**, D457-62.

Bear, J., Tan, W., Zolotukhin, A. S., Tabernero, C., Hudson, E. A. and Felber, B. K. (1999). Identification of Novel Import and Export Signals of Human TAP, the Protein That Binds to the Constitutive Transport Element of the Type D Retrovirus mRNAs. *Mol. Cell. Biol.* **19**, 6306–6317.

Ben-Yishay, R., Mor, A., Shraga, A., Ashkenazy-Titelman, A., Kinor, N., Schwed-Gross, A., Jacob, A., Kozer, N., Kumar, P., Garini, Y., et al. (2019). Imaging within single NPCs reveals NXF1's role in mRNA export on the cytoplasmic side of the pore. *J. Cell Biol.* **218**, 2962–2981.

Billington, K., Halliday, C., Madden, R., Dyer, P., Barker, A. R., Moreira-Leite, F. F., Carrington, M., Vaughan, S., Hertz-Fowler, C., Dean, S., et al. (2023). Genome-wide subcellular protein map for the flagellate parasite Trypanosoma brucei. *Nat. Microbiol.* **8**, 533–547.

Branon, T. C., Bosch, J. A., Sanchez, A. D., Udeshi, N. D., Svinkina, T., Carr, S. A., Feldman, J. L., Perrimon, N. and Ting, A. Y. (2018). Efficient proximity labeling in living cells and organisms with TurboID. *Nature biotechnology* **36**, 880–887.

Brun, R. and Schönenberger (1979). Cultivation and in vitro cloning or procyclic culture forms of Trypanosoma brucei in a semi-defined medium. Short communication. *Acta tropica* **36**, 289–292.

Chakraborty, P. and Zweckstetter, M. (2023). Role of aberrant phase separation in pathological protein aggregation. *Curr. Opin. Struct. Biol.* **82**, 102678.

Chen, F., Tillberg, P. W. and Boyden, E. S. (2015). Expansion microscopy. *Science* **347**, 543–548.

Chen, R., Zhang, N., Zhou, Y. and Jing, J. (2022). Optical Sensors and Actuators for Probing Proximity-Dependent Biotinylation in Living Cells. *Front Cell Neurosci* **16**, 801644.

Chivers, C. E., Koner, A. L., Lowe, E. D. and Howarth, M. (2011). How the biotin–streptavidin interaction was made even stronger: investigation via crystallography and a chimaeric tetramer. *Biochem. J.* **435**, 55–63.

Cho, K. F., Branon, T. C., Rajeev, S., Svinkina, T., Udeshi, N. D., Thoudam, T., Kwak, C., Rhee, H.-W., Lee, I.-K., Carr, S. A., et al. (2020). Split-TurboID enables contact-dependent proximity labeling in cells. *Proc National Acad Sci* **117**, 12143–12154.

Chu, X., Sun, T., Li, Q., Xu, Y., Zhang, Z., Lai, L. and Pei, J. (2022). Prediction of liquid–liquid phase separating proteins using machine learning. *BMC Bioinform.* **23**, 72.

Cox, J. and Mann, M. (2008). MaxQuant enables high peptide identification rates, individualized p.p.b.-range mass accuracies and proteome-wide protein quantification. *Nature biotechnology* **26**, 1367–1372.

Cox, J., Hein, M. Y., Luber, C. A., Paron, I., Nagaraj, N. and Mann, M. (2014). Accurate Proteome-wide Label-free Quantification by Delayed Normalization and Maximal Peptide Ratio Extraction, Termed MaxLFQ*. *Mol Cell Proteomics* **13**, 2513–2526.

Dai, Z. and Yang, X. (2023). The regulation of liquid-liquid phase separated condensates containing nucleic acids. *FEBS J.*

Davis, L. K., Ford, I. J. and Hoogenboom, B. W. (2022). Crowding-induced phase separation of nuclear transport receptors in FG nucleoporin assemblies. *eLife* **11**, e72627.

Dean, S., Sunter, J., Wheeler, R. J., Hodkinson, I., Gluenz, E. and Gull, K. (2015). A toolkit enabling efficient, scalable and reproducible gene tagging in trypanosomatids. *Open biology* **5**, 140197.

Derrer, C. P., Mancini, R., Vallotton, P., Huet, S., Weis, K. and Dultz, E. (2019). The RNA export factor Mex67 functions as a mobile nucleoporin. *The Journal of Cell Biology* **218**, 3967–3976.

Dostalova, A., Käser, S., Cristodero, M. and Schimanski, B. (2013). The nuclear mRNA export receptor Mex67-Mtr2 of Trypanosoma brucei contains a unique and essential zinc finger motif. *Molecular Microbiology* **88**, 728–739.

Fritz, M., Vanselow, J., Sauer, N., Lamer, S., Goos, C., Siegel, T. N., Subota, I., Schlosser, A., Carrington, M. and Kramer, S. (2015). Novel insights into RNP granules by employing the trypanosome's microtubule skeleton as a molecular sieve. *Nucleic Acids Research* **43**, 8013–8032.

Gambarotto, D., Zwettler, F. U., Guennec, M. L., Schmidt-Cernohorska, M., Fortun, D., Borgers, S., Heine, J., Schloetel, J. G., Reuss, M., Unser, M., et al. (2019). Imaging cellular ultrastructures using expansion microscopy (U-ExM). *Nat Methods* **16**, 71–74.

Gambarotto, D., Hamel, V. and Guichard, P. (2020). Ultrastructure expansion microscopy (U-ExM). *Methods Cell Biol* **161**, 57–81.

Holden, J. M., Koreny, L., Obado, S., Ratushny, A. V., Chen, W. M., Chiang, J. H., Kelly, S., Chait, B. T., Aitchison, J. D., Rout, M. P., et al. (2014). Nuclear pore complex evolution: a

865 trypanosome Mlp analogue functions in chromosomal segregation but lacks
866 transcriptional barrier activity. *Molecular biology of the cell* **25**, 1421–1436.

867 **Katahira, J., Strässer, K., Podtelejnikov, A., Mann, M., Jung, J. U. and Hurt, E.** (1999). The
868 Mex67p-mediated nuclear mRNA export pathway is conserved from yeast to human. *The*
869 *EMBO journal* **18**, 2593–2609.

870 **Kelly, S., Reed, J., Kramer, S., Ellis, L., Webb, H., Sunter, J., Salje, J., Marinsek, N., Gull, K.,**
871 **Wickstead, B., et al.** (2007). Functional genomics in Trypanosoma brucei: a collection of
872 vectors for the expression of tagged proteins from endogenous and ectopic gene loci.
873 *Molecular & Biochemical Parasitology* **154**, 103–109.

874 **Kim, D. I., Birendra, K. C., Zhu, W., Motamedchaboki, K., Doye, V. and Roux, K. J.** (2014).
875 Probing nuclear pore complex architecture with proximity-dependent biotinylation.
876 *Proceedings of the National Academy of Sciences of the United States of America* **111**,
877 E2453-61.

878 **Kim, D. I., Jensen, S. C., Noble, K. A., KC, B., Roux, K. H., Motamedchaboki, K. and Roux, K.**
879 **J.** (2016). An improved smaller biotin ligase for BioID proximity labeling. *Mol. Biology Cell*
880 **27**, 1188–1196.

881 **Köhler, A. and Hurt, E.** (2007). Exporting RNA from the nucleus to the cytoplasm. *Nature*
882 *Reviews Molecular Cell Biology* **8**, 761–773.

883 **Kramer, S.** (2017). The ApaH-like phosphatase TbALPH1 is the major mRNA decapping
884 enzyme of trypanosomes. *PLoS Pathogens* **13**, e1006456.

885 **Kramer, S., Queiroz, R., Ellis, L., Webb, H., Hoheisel, J. D., Clayton, C. E. and Carrington, M.**
886 (2008). Heat shock causes a decrease in polysomes and the appearance of stress granules
887 in trypanosomes independently of eIF2(alpha) phosphorylation at Thr169. *Journal of Cell*
888 *Science* **121**, 3002–3014.

889 **Kramer, S., Kimblin, N. C. and Carrington, M.** (2010). Genome-wide in silico screen for
890 CCCH-type zinc finger proteins of Trypanosoma brucei, Trypanosoma cruzi and
891 Leishmania major. *BMC genomics* **11**, 283.

892 **Kramer, S., Bannerman-Chukualim, B., Ellis, L., Boulden, E. A., Kelly, S., Field, M. C. and**
893 **Carrington, M.** (2013). Differential Localization of the Two T. brucei Poly(A) Binding
894 Proteins to the Nucleus and RNP Granules Suggests Binding to Distinct mRNA Pools. *PLoS*
895 *ONE* **8**, e54004.

896 **Kramer, S., Meyer-Natus, E., Stigloher, C., Thoma, H., Schnaufer, A. and Engstler, M.**
897 (2020). Parallel monitoring of RNA abundance, localization and compactness with
898 correlative single molecule FISH on LR White embedded samples. *Nucleic Acids Res* **49**,
899 gkaa1142-.

Kramer, S., Karolak, N. K., Odenwald, J., Gabiatti, B., Londoño, P. A. C., Zavřelová, A., Freire, E. R., Almeida, K. S., Braune, S., Moreira, C., et al. (2023). A unique mRNA decapping complex in trypanosomes. *Nucleic Acids Res.* **51**, 7520–7540.

Laitinen, O. H., Hytönen, V. P., Nordlund, H. R. and Kulomaa, M. S. (2006). Genetically engineered avidins and streptavidins. *Cell. Mol. Life Sci. CMLS* **63**, 2992–3017.

Luong, J. H. T. and Vashist, S. K. (2020). Chemistry of Biotin–Streptavidin and the Growing Concern of an Emerging Biotin Interference in Clinical Immunoassays. *ACS Omega* **5**, 10–18.

Mangus, D. A., Evans, M. C. and Jacobson, A. (2003). Poly(A)-binding proteins: multifunctional scaffolds for the post-transcriptional control of gene expression. *Genome biology* **4**, 223.

May, D. G., Scott, K. L., Campos, A. R. and Roux, K. J. (2020). Comparative Application of BioID and TurboID for Protein-Proximity Biotinylation. *Cells* **9**, 1070.

McCulloch, R., Vassella, E., Burton, P., Boshart, M. and Barry, J. D. (2004). Transformation of monomorphic and pleomorphic Trypanosoma brucei. *Methods in molecular biology (Clifton, NJ)* **262**, 53–86.

Misteli, T. (2008). Physiological importance of RNA and protein mobility in the cell nucleus. *Histochem. Cell Biol.* **129**, 5–11.

Moreira, C. M. do N., Kelemen, C. D., Obado, S. O., Zahedifard, F., Zhang, N., Holetz, F. B., Gauglitz, L., Dallagiovanna, B., Field, M. C., Kramer, S., et al. (2023). Impact of inherent biases built into proteomic techniques: Proximity labeling and affinity capture compared. *J Biol Chem* **299**, 102726.

Morelle, C., Sterkers, Y., Crobu, L., MBang-Benet, D. E., Kuk, N., Portalès, P., Bastien, P., Pagès, M. and Lachaud, L. (2015). The nucleoporin Mlp2 is involved in chromosomal distribution during mitosis in trypanosomatids. *Nucleic Acids Research* **43**, 4013–4027.

Musinova, Y. R., Lisitsyna, O. M., Golyshev, S. A., Tuzhikov, A. I., Polyakov, V. Y. and Sheval, E. V. (2011). Nucleolar localization/retention signal is responsible for transient accumulation of histone H2B in the nucleolus through electrostatic interactions. *Biochim. Biophys. Acta (BBA) - Mol. Cell Res.* **1813**, 27–38.

Nag, N., Sasidharan, S., Uversky, V. N., Saudagar, P. and Tripathi, T. (2022). Phase separation of FG-nucleoporins in nuclear pore complexes. *Biochimica Et Biophysica Acta Bba - Mol Cell Res* **1869**, 119205.

Neuhaus, E. M., Horstmann, H., Almers, W., Maniak, M. and Soldati, T. (1998). Ethane-Freezing/Methanol-Fixation of Cell Monolayers: A Procedure for Improved Preservation of Structure and Antigenicity for Light and Electron Microscopies. *J. Struct. Biol.* **121**, 326–342.

Obado, S. O., Brillantes, M., Uryu, K., Zhang, W., Ketaren, N. E., Chait, B. T., Field, M. C. and Rout, M. P. (2016). Interactome Mapping Reveals the Evolutionary History of the Nuclear Pore Complex. *PLoS biology* **14**, e1002365.

Ong, J. Y. and Torres, J. Z. (2020). Phase Separation in Cell Division. *Mol Cell* **80**, 9–20.

Perez-Riverol, Y., Csordas, A., Bai, J., Bernal-Llinares, M., Hewapathirana, S., Kundu, D. J., Inuganti, A., Griss, J., Mayer, G., Eisenacher, M., et al. (2019). The PRIDE database and related tools and resources in 2019: improving support for quantification data. *Nucleic Acids Research* **47**, D442–D450.

Piña, R., Santos-Díaz, A. I., Orta-Salazar, E., Aguilar-Vazquez, A. R., Mantellero, C. A., Acosta-Galeana, I., Estrada-Mondragon, A., Prior-Gonzalez, M., Martinez-Cruz, J. I. and Rosas-Arellano, A. (2022). Ten Approaches That Improve Immunostaining: A Review of the Latest Advances for the Optimization of Immunofluorescence. *Int. J. Mol. Sci.* **23**, 1426.

Pozzi, B., Naguleswaran, A., Florini, F., Rezaei, Z. and Roditi, I. (2023). The RNA export factor TbMex67 connects transcription and RNA export in Trypanosoma brucei and sets boundaries for RNA polymerase I. *Nucleic Acids Res.* **51**, 5177–5192.

Rappsilber, J., Mann, M. and Ishihama, Y. (2007). Protocol for micro-purification, enrichment, pre-fractionation and storage of peptides for proteomics using StageTips. *Nat Protoc* **2**, 1896–1906.

Rodriguez, M. S., Dargemont, C. and Stutz, F. (2004). Nuclear export of RNA. *Biol. Cell* **96**, 639–655.

Schwede, A., Manful, T., Jha, B. A., Helbig, C., Bercovich, N., Stewart, M. and Clayton, C. E. (2009). The role of deadenylation in the degradation of unstable mRNAs in trypanosomes. *Nucleic Acids Research* **37**, 5511–5528.

Shafraz, O., Davis, C. M. O. and Sivasankar, S. (2023). Light Activated BioID (LAB): an optically activated proximity labeling system to study protein-protein interactions. *J. Cell Sci.* **136**, jcs261430.

Sherwin, T. and Gull, K. (1989). Visualization of detyrosination along single microtubules reveals novel mechanisms of assembly during cytoskeletal duplication in trypanosomes. *Cell* **57**, 211–221.

Sheval, E. V., Polzikov, M. A., Olson, M. O. J. and Zatsepina, O. V. (2005). A higher concentration of an antigen within the nucleolus may prevent its proper recognition by specific antibodies. *Eur. J. Histochem. : EJH* **49**, 117–23.

So, C., Cheng, S. and Schuh, M. (2021). Phase Separation during Germline Development. *Trends Cell Biol.* **31**, 254–268.

Stewart, M. (2019). Polyadenylation and nuclear export of mRNAs. *Journal of Biological Chemistry* **294**, 2977–2987.

Sträßer, K., Baßler, J. and Hurt, E. (2000). Binding of the Mex67p/Mtr2p Heterodimer to Fxfg, Glfg, and Fg Repeat Nucleoporins Is Essential for Nuclear mRNA Export. *J. Cell Biol.* **150**, 695–706.

Sunter, J., Wickstead, B., Gull, K. and Carrington, M. (2012). A new generation of T7 RNA polymerase-independent inducible expression plasmids for Trypanosoma brucei. *PLoS ONE* **7**, e35167.

Svistunova, D. M., Musinova, Y. R., Polyakov, V. Yu. and Sheval, E. V. (2011). A Simple Method for the Immunocytochemical Detection of Proteins Inside Nuclear Structures That Are Inaccessible to Specific Antibodies. *J. Histochem. Cytochem.* **60**, 152–158.

Terry, L. J. and Wente, S. R. (2007). Nuclear mRNA export requires specific FG nucleoporins for translocation through the nuclear pore complex. *J. Cell Biol.* **178**, 1121–1132.

Tillberg, P. W., Chen, F., Piatkevich, K. D., Zhao, Y., Yu, C.-C. (Jay), English, B. P., Gao, L., Martorell, A., Suk, H.-J., Yoshida, F., et al. (2016). Protein-retention expansion microscopy of cells and tissues labeled using standard fluorescent proteins and antibodies. *Nat. Biotechnol.* **34**, 987–992.

Tinti, M. and Ferguson, M. A. J. (2022). Visualisation of proteome-wide ordered protein abundances in Trypanosoma brucei. *Wellcome Open Res.* **7**, 34.

Tsoi, P. S., Quan, M. D., Ferreon, J. C. and Ferreon, A. C. M. (2023). Aggregation of Disordered Proteins Associated with Neurodegeneration. *Int. J. Mol. Sci.* **24**, 3380.

Tyanova, S., Temu, T., Sinitcyn, P., Carlson, A., Hein, M. Y., Geiger, T., Mann, M. and Cox, J. (2016). The Perseus computational platform for comprehensive analysis of (prote)omics data. *Nature methods* **13**, 731–740.

Venko, K. and Žerovnik, E. (2023). Protein Condensates and Protein Aggregates: In Vitro, in the Cell, and In Silico. *Front. Biosci.-Landmark* **28**, 183.

Youn, J.-Y., Dunham, W. H., Hong, S. J., Knight, J. D. R., Bashkurov, M., Chen, G. I., Bagci, H., Rathod, B., MacLeod, G., Eng, S. W. M., et al. (2018). High-Density Proximity Mapping Reveals the Subcellular Organization of mRNA-Associated Granules and Bodies. *Mol. Cell* **69**, 517-532.e11.

Zatsepina, O. V., Todorov, I. T., Philipova, R. N., Krachmarov, C. P., Trendelenburg, M. F. and Jordan, E. G. (1997). Cell cycle-dependent translocations of a major nucleolar phosphoprotein, B23, and some characteristics of its variants. *Eur. J. cell Biol.* **73**, 58–70.

Zhang, Y. and Shen, L. (2023). An in vitro Assay to Probe the Formation of Biomolecular Condensates. *Bio-Protoc.* **13**, e4813.

1006

Figure 1

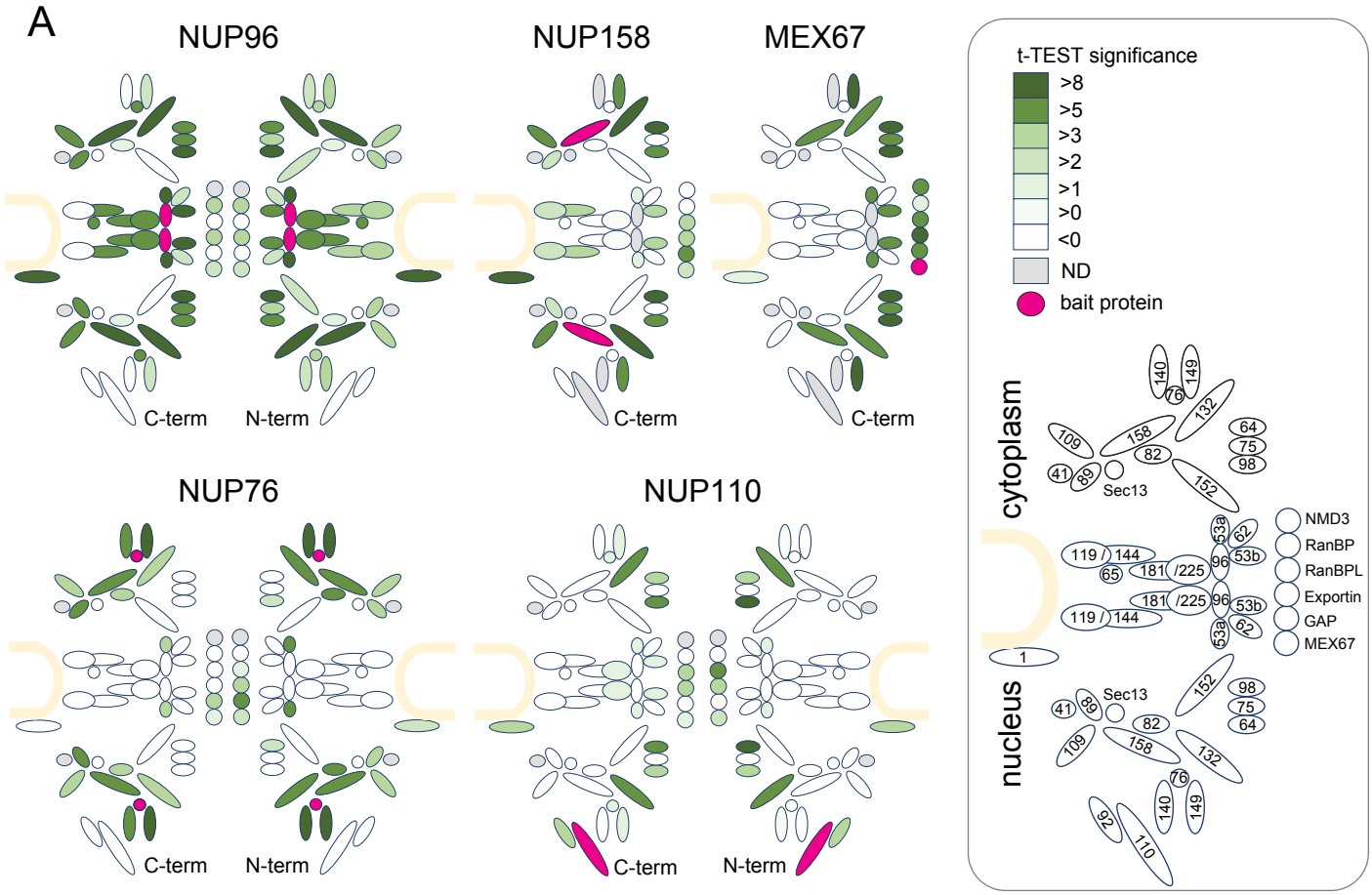

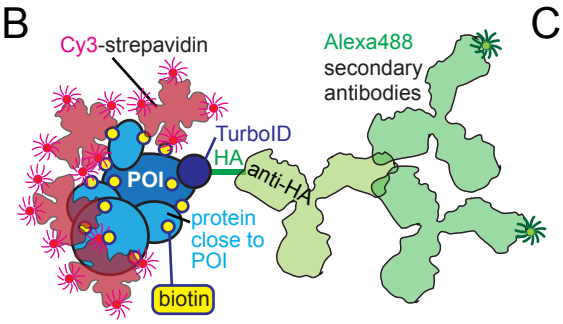

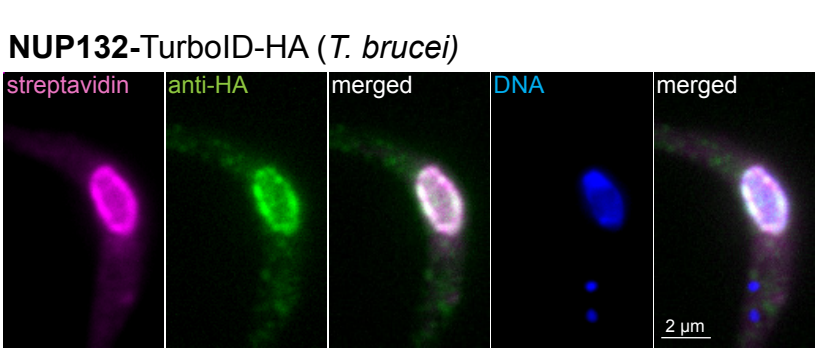

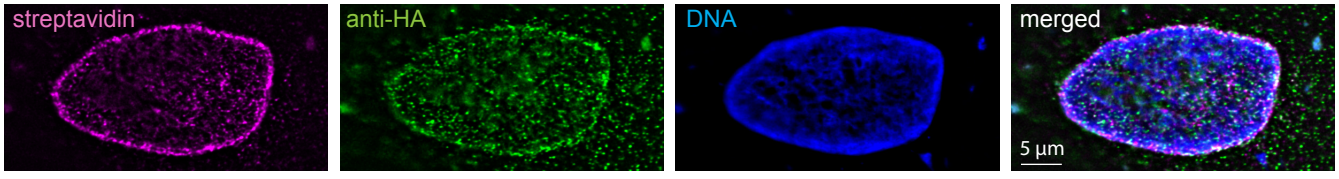

Figure 2

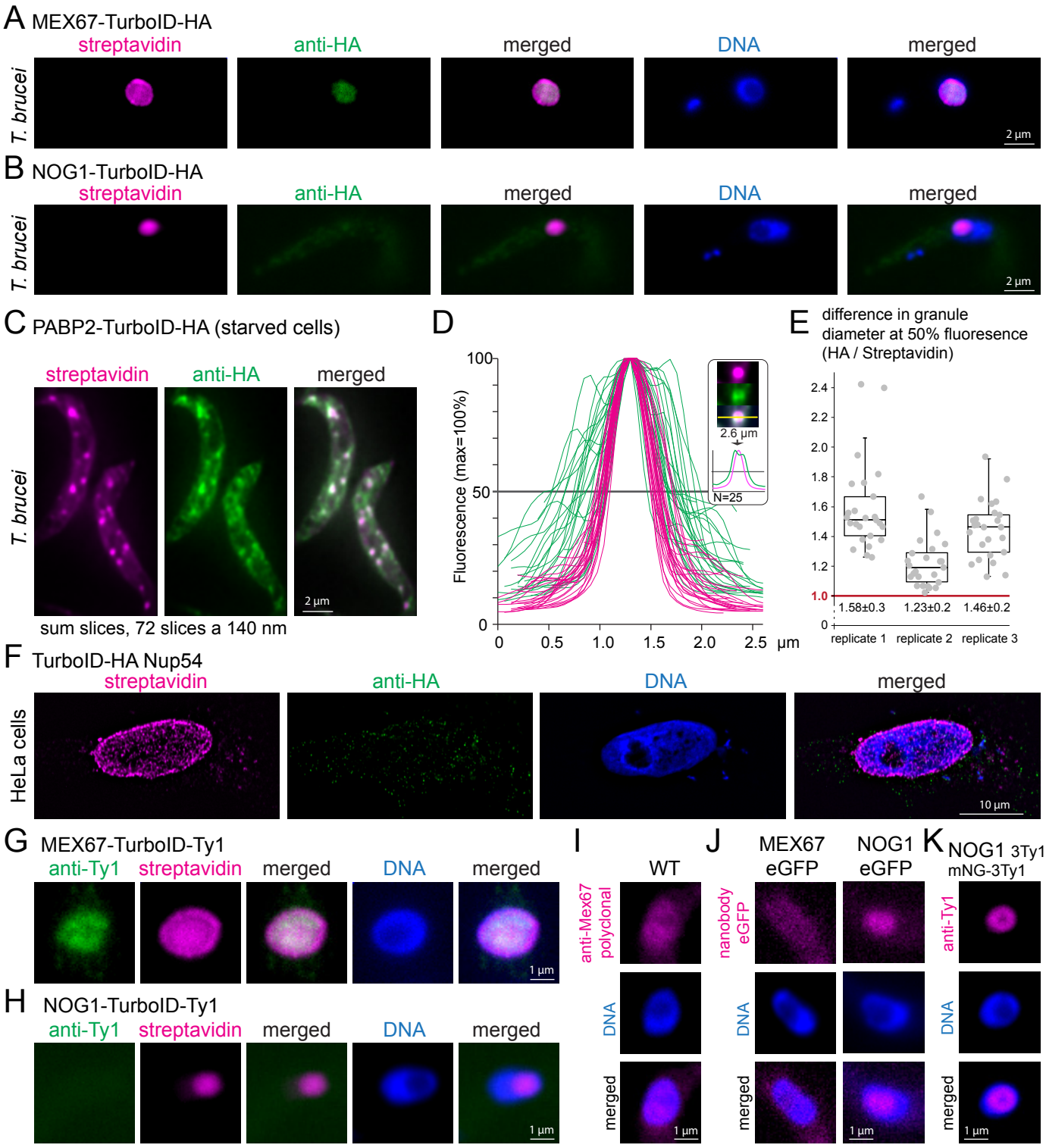

Figure 3

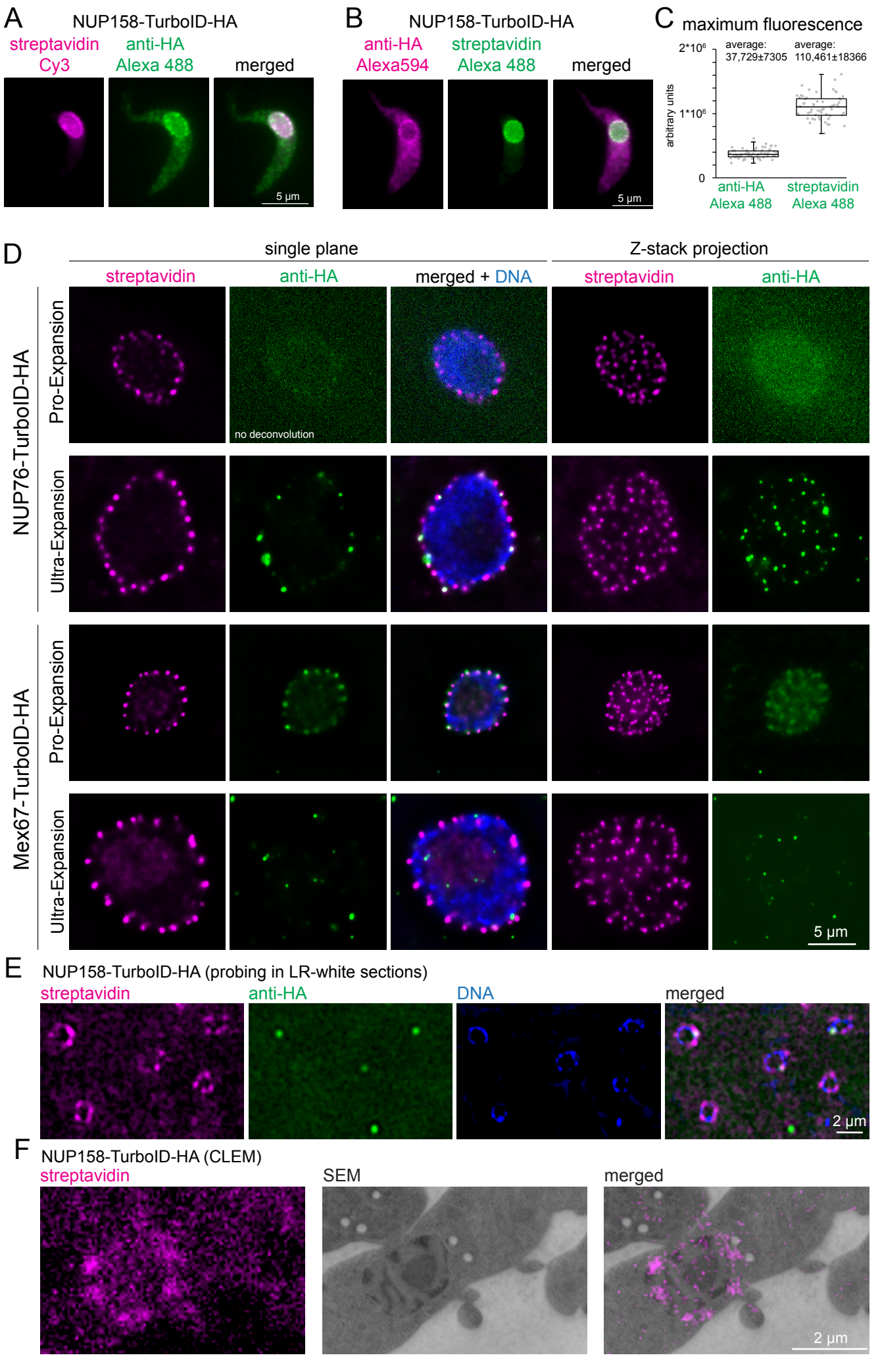

Figure 4

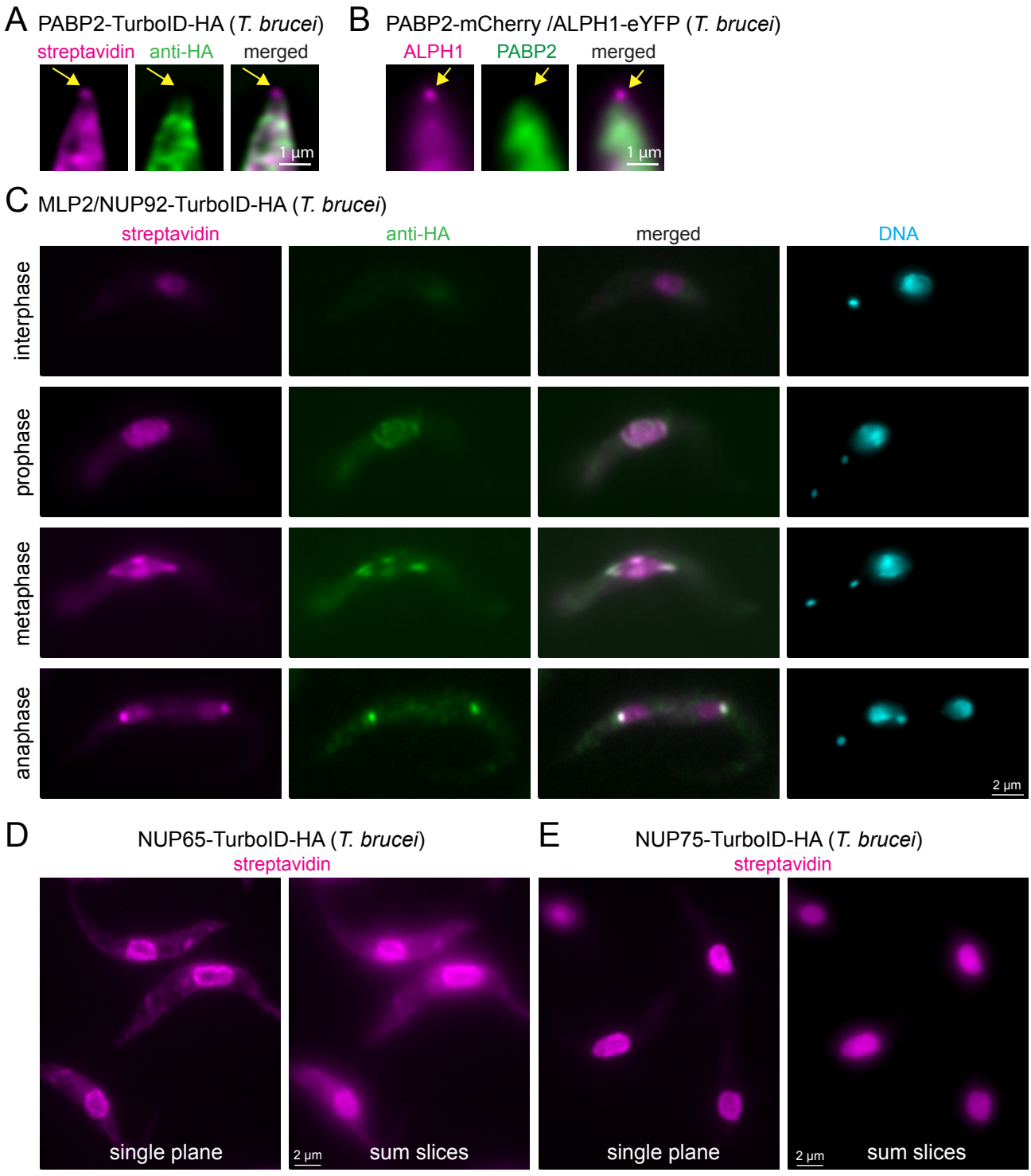

Figure 5